The effects of drainage conditions on liquefaction response of slopes and the inference for lifelines

Ehsanollah Atigh
Department of Civil Engineering, University of British Columbia, Vancouver, B.C.

Peter M. Byrne
Department of Civil Engineering, University of British Columbia, Vancouver, B.C.

Abstract: Lifeline structures commonly traverse slopes underlain by liquefiable soils. The effect of such liquefaction can be to impose large forces or displacements on the lifeline. The structure may be designed or retrofitted to accommodate such loading or the soil may be remediated to prevent or curtail liquefaction. In either case the post-liquefaction response of the soil is required. In current design practice this is based on the assumption that the soil responds in an undrained manner. Laboratory test data and analyses are presented to illustrate that this may not be a conservative assumption, particularly where drainage is curtailed by the presence of low permeability layers. Such layers are commonly encountered in practice, and it is important that they be identified. Shaking table tests as well as field experience confirm that curtailment of drainage can lead to a much more severe condition than the undrained state commonly assumed, and consequently this should be considered in design.

Introduction

Lifelines commonly traverse or cross slopes susceptible to liquefaction, particularly in the Lower Mainland region of British Columbia. Specific examples are the water pipeline and bridge crossings at First and Second Narrows in Burrard Inlet and the many bridge crossings on the Fraser River including those at Oak Street and Port Mann.

The concerns for lifeline structures that are embedded in soil that may liquefy are: (1) loss of soil strength; and (2) possible large soil displacements. If the structure is relying on soil support such as from end bearing piles, then loss of strength can cause the piles to plunge and this would normally result in very severe damage. If, on the other hand, the pile tips are adequately supported below the depth of liquefaction, the concern would be that lateral soil movements associated with liquefaction could drag on the structures and result in excessive lateral force or displacement. Liquefaction-induced soil displacements are, therefore, a major concern in design or retrofit of lifeline structures.

In dealing with liquefaction there are essentially three concerns:

1) Will the design earthquake trigger liquefaction in significant zones, and if so,
2) Will large movements associated with a flow slide occur, and if not,
3) What displacements and forces on the structure may occur?

These concerns are now commonly addressed with a single synthesized analysis such as that proposed by Beaty and Byrne (1999,2000), and this or similar approaches have recently been used on a number of lifeline structures including Port Mann and Oak Street Bridges, and water pipeline crossings at First and Second Narrows.

In all such analyses carried out to date, it has been assumed that because earthquake loading is very rapid, there will be little time for drainage to occur and triggering of liquefaction will occur in an undrained state. In addition, when examining stability and deformation after liquefaction has been triggered, it is generally assumed that the post-triggering soil response, and in particular the residual strength, is also undrained.

Recent test data reported by Vaid and Sivathayalan (1998) and Eliadorani (2000) indicate that a very small inflow of water into a soil element as it is being sheared can cause a very large reduction in strength and stiffness compared to an undrained state. This finding is particularly important in assessing the stability of slopes underlain by stratified deposits in which vertical drainage is impeded.

The earthquake induced slope failure on the upstream side of the Lower San Fernando Dam in 1971 occurred some time after the shaking, and indicates that while the residual strength in liquefied zones was adequate to prevent a flow slide during shaking, a loss in strength consistent with inflow occuring some time later. The Lower San Fernando Dam had been constructed by hydraulic placement and was highly stratified.

Shaking table tests presented by Kokushu (1998) on submerged granular slopes show that an accumulation of water (water bubble) occurs beneath a drainage barrier layer and results in a flow slide after shaking has ceased.

The purpose of this paper is to illustrate the effect of drainage barrier layers on the stability of slopes using numerical modelling and the laboratory data of Eliadorani on Fraser River sand.

Shear behaviour of Fraser River sand when subjected to inflow

A comprehensive series of laboratory test data on Fraser River sand are reported by Eliadorani (2000). Drained, undrained as well as "inflow" tests were carried out in both extension and compression modes. The tests were performed mostly on loose sand with relative density, D_r=30%, although some denser states were also examined. The effective confining stress prior to shearing ranged between 20 kPa and 400 kPa.

Inflow shear loading was simulated using a constant ratio of volumetric strain increment to axial strain increment, $d\varepsilon_v/d\varepsilon_1$, while the radial total stress was held constant. The increment of volume change, $d\varepsilon_v$ was controlled by inflow of water into the sample. The prescribed strain increments result in an effective stress change, and this is reflected in the change in water pressure or element pore pressure required to cause the required volume change. The soil specimen was subjected to a constant strain increment ratio path using the increment in axial deformation as the control variable. A wide range of strain increment ratio was used. The undrained test is a special case in which $d\varepsilon_v$=0.

The results of undrained and inflow tests for dense Fraser River sand are presented in Fig. 1. The dense sand when tested undrained is strongly dilatant and strain hardening in its response. The inflow test in which $d\varepsilon_v/d\varepsilon_1$ = -0.6 (expansion) is strain hardening initially, but after an axial strain of only 0.2% commences to strain soften and at 4% has negligible strength. Thus, inflow of a very small amount of water into a dense strain hardening sample can turn it into a weak strain softening material.

The effect of inflow on stress-strain response of a loose sample is shown in Fig. 2. The loose sample when tested undrained is mildly dilative. When subjected to inflow at a rate $d\varepsilon_v/d\varepsilon_1$ = -1, it becomes strongly strain softening and after 1.5% axial strain has zero strength.

The effective stress paths followed for undrained and inflow conditions for a dense sample are shown in Fig. 3. It may be seen that the small inflow volume greatly reduces the normal effective stress, and drives the stress point back to the origin.

The results presented in Figs. 1, 2 and 3, show that strain softening can be triggered in loose as well as dense sands at strains of about 0.2% by the inflow of only a small volume of water. Residual strengths close to zero are reached for inflow volumetric strains of 1%-2%.

In a field event, a wide range of volumetric strains can occur in soil elements during dissipation of generated excess pore water pressure arising from monotonic or earthquake loading. Generally, outflow from elements would be expected, but if flow of water is blocked due to a less permeable layer, inflow can occur in the nearby elements. This will result in a much softer response in

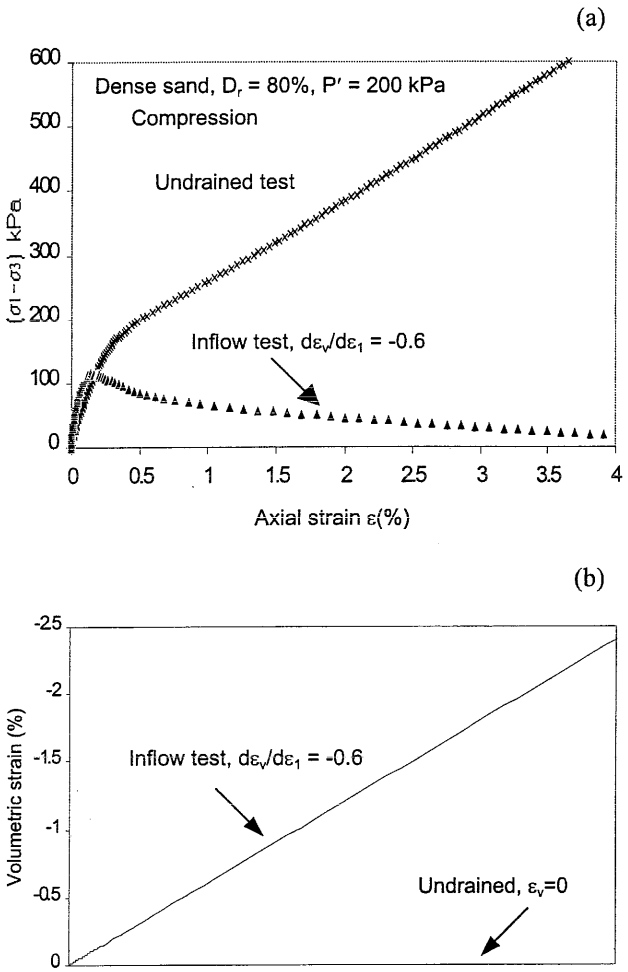

Fig. 1. Stress strain response of dense Fraser River sand in undrained and inflow triaxial tests, (modified from Eliadorani, 2000): (a) Stress strain response, (b) Volumetric strain versus axial strain

these elements, due to reduced effective stresses, and may lead to a flow failure of the slope.

In order to investigate this phenomenon, a stress-strain model that can capture the sand responses in drained as well as controlled inflow and outflow conditions is required. The stress strain model used in this study is discussed and its ability to predict sand response under different drainage conditions verified. The model is then used to analyze the behavior of an embankment taking into account dissipation of excess pore water pressure under a range of drainage conditions.

Stress strain model for sand liquefaction

The constitutive model for sand used in this study is based on an elasto-plastic stress strain relationship. The model was initially proposed by Byrne et al. (1995) and has been

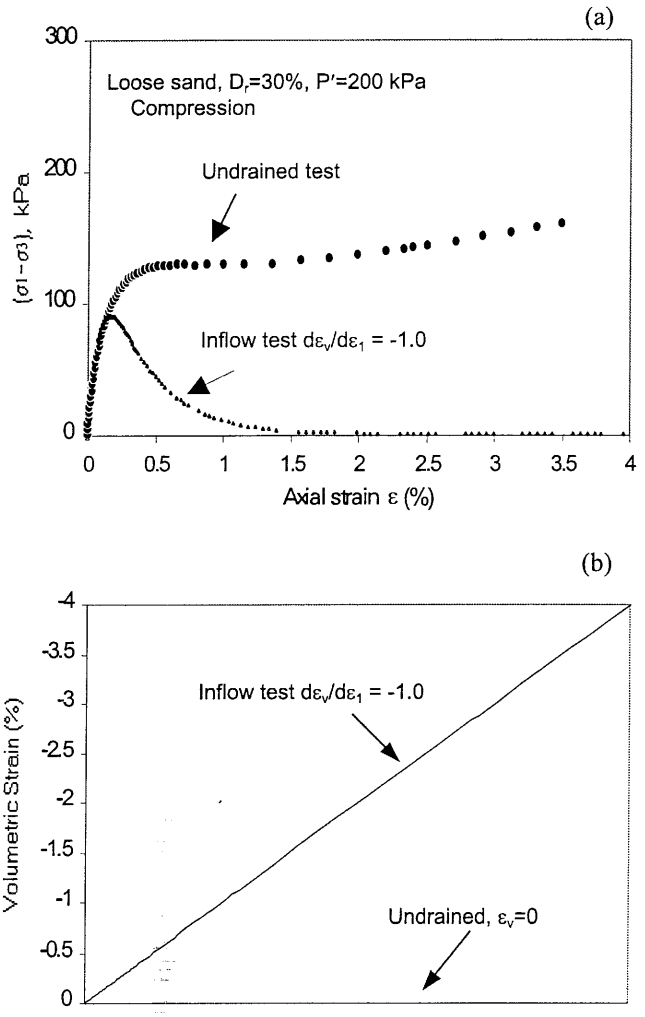

Fig. 2. Stress strain response of loose Fraser River sand in undrained and inflow triaxial tests, (Eliadorani, 2000): (a) Stress strain response, (b) Volumetric strain versus axial strain

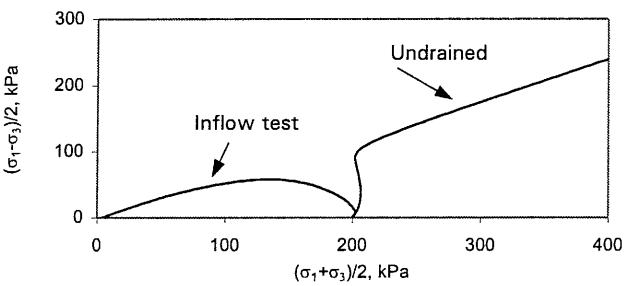

Fig. 3. Effective stress paths for undrained and inflow tests.

further developed by Puebla et al. (1997). The basic concepts of the model have been presented in detail by Puebla (1999) and are briefly described here. It is an incremental elastic-plastic model in which the yield loci are lines of constant stress ratio or developed friction angle. The flow rule relating plastic strain increment directions is non associated and leads to a plastic potential defined in terms of dilation angle ψ as shown in Fig. 4.

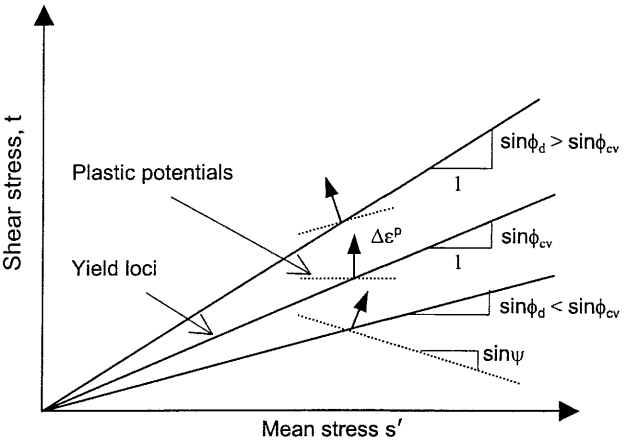

Fig. 4. Yield loci, plastic potentials, and plastic strain increment vectors

Plastic shear strain is the hardener that allows the yield locus to expand or stress ratio, $\eta = \sin\phi_d$, to increase. The plastic shear strain increment for any increase in stress ratio, $\Delta\eta$, is shown in Fig. 5.

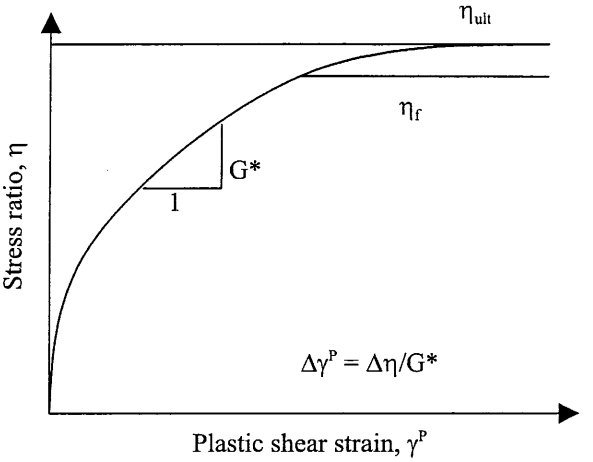

Fig. 5. Hyperbolic relation between stress ratio η and plastic shear strain γ^p

The *elastic* response is assumed to be incremental linear and isotropic and is specified by two elastic parameters; the shear modulus, G^e and Poisson's ratio, μ. G^e is assumed to be stress level dependent as follows:

$$[1] \qquad G^e = K_G^e P_A \left(\frac{s'}{P_A}\right)^{ne}$$

in which;

K_G^e : elastic shear modulus number
ne : elastic shear modulus exponent
P_A : atmospheric pressure in specified units
s′ : mean effective stress; $s'=(\sigma'_1+\sigma'_3)/2$; σ'_1 and σ'_3 are major and minor principal effective stresses, respectively.

Poisson's ratio is assumed constant and equal to 0.125.

The plastic shear strain increment, $\Delta\gamma^p$ is obtained from the normalized tangent plastic shear modulus G^* (shown in Fig. 5), and the stress ratio increment, $\Delta\eta$, as follows:

$$[2] \quad \Delta\gamma^p = \left(\frac{1}{G^*}\right)\Delta\eta$$

when

$$[3] \quad \Delta\eta = \left[\frac{\Delta t}{s'} - \left(\frac{\eta_d}{s'}\right)\Delta s'\right]$$

and

$$[4] \quad G^* = K_G^p\left(\frac{s'}{P_A}\right)^{np-1}\left[1-\left(\frac{\eta_d}{\eta_f}\right)R_f\right]^2$$

In which
K_G^p : plastic shear modulus number
np : plastic shear modulus exponent
η_f : stress ratio at failure, as shown in Fig. 5
R_f : failure ratio = η_F/η_{ult}; η_{ult} is the ultimate stress ratio from the best-fit hyperbola, as shown in Fig. 5.
η_d : developed stress ratio = sin ϕ_d; ϕ_d is the developed friction angle
t : $(\sigma_1-\sigma_3)/2$
s : $(\sigma'_1+\sigma'_3)/2$

The plastic volumetric strain increment $\Delta\varepsilon_v^p$ is obtained from the flow rule:

$$[5] \quad \Delta\varepsilon_v^p = (\sin\psi)\,\Delta\gamma^p$$

Where ψ is the dilation angle, which is related to the constant volume friction angle ϕ_{cv} and the developed friction angle ϕ_d by:

$$[6] \quad \sin\psi = (\sin\phi_{cv} - \sin\phi_d)$$

The total response is the sum of elastic and plastic components and it can be written in matrix form:

$$[7] \quad \{\Delta\sigma'\} = [D']\{\Delta\varepsilon\}$$

in which:

$\{\Delta\sigma'\}$ is the effective stress increment vector
$[D']$ is the constitutive model matrix in terms of effective stresses
$\{\Delta\varepsilon\}$ is the vector of total strain increments, plastic and elastic.

Numerical analysis procedure

Numerical analysis of a stress-deformation problem requires that equilibrium and compatibility be satisfied for the boundary conditions using an appropriate stress strain model. Two different techniques are commonly used; finite element and finite difference methods. In this study, the analyses were carried out using the computer code FLAC (Fast Lagrangian Analysis of Continua), version 3.4 (Cundall, 1998). FLAC uses a finite difference method and satisfies dynamic equilibrium using a step-by-step explicit time domain procedure. The soil body is divided into a finite mesh composed of quadrilateral elements. Even though the program is used to find a static solution to a problem, the dynamic equations of motion are included in the formulation. One advantage of this approach is that the solution is numerically stable even when the problem is not statically stable.

The program provides the ability for users to implement their own constitutive model. The described stress strain model has been implemented in FLAC and is used in the analyses. FLAC can be used to model the stress-deformation problem alone (including drained, undrained or prescribed volume changes), the flow problem alone, or coupled stress flow.

The analysis procedure is first applied to the test data to assure that it can capture the range of sand response from drained, to undrained, to inflow states. It is then applied to an embankment where the effect of impeded drainage is examined.

Simulation of element tests

Analyses were performed using the described stress-strain model to simulate the tests on loose Fraser River sand as obtained by Eliadorani (2000). The calibration of the model was carried out using the results of conventional drained triaxial compression tests by analyzing a single element of soil. The model parameters so obtained were then used to predict the undrained and inflow responses.

The predicted and observed responses of loose sand in conventional drained triaxial compression tests for different confining pressures are shown in Fig. 6 (Eliadorani, 2000). The model parameters were adjusted to obtain the best fit to the laboratory data and resulting predictions are also shown in Fig. 6 for comparison. It may be seen that the predicted and observed $(\sigma_1-\sigma_3)$ vs axial strain data are in very close agreement. The

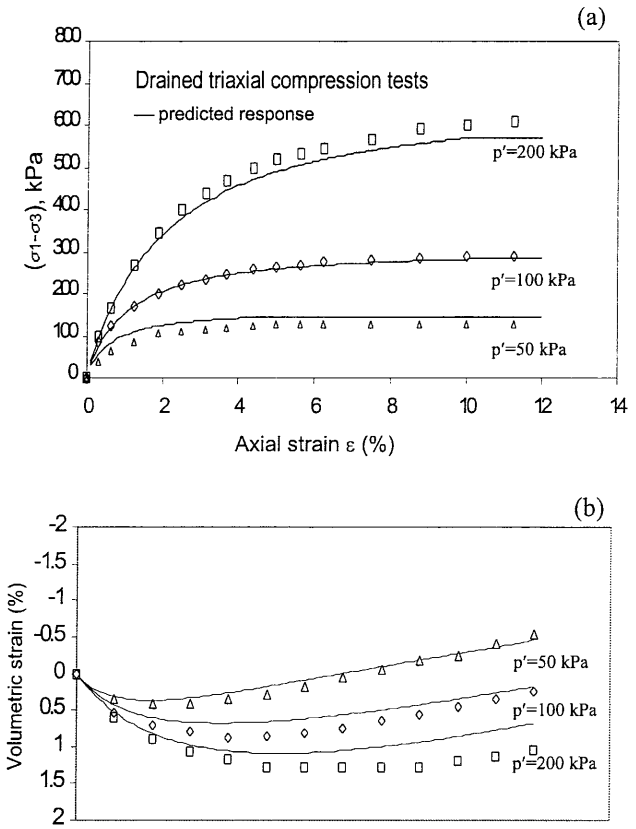

Fig. 6. Measured and predicted element response of loose Fraser River sand: (a) Stress-strain response, (b) Volumetric strain versus axial strain.

predicted and observed volumetric strain vs axial strain is in very good agreement for the confining stress of 50 kPa. The agreement is not as good for a confining stress of 200 kPa at higher strains. The model parameters used to obtain this fit are listed in Table 1 for loose Fraser River sand. The plastic anisotropy factor allowed both compression and extension test data to be captured.

Table 1. Model parameters used for analysis

Parameters	
Elastic shear modulus number, K_G^e	300
Elastic shear modulus exponent, n_e	0.25
Elastic Poisson's ratio	0.125
Plastic shear modulus number, K_G^p	340
Plastic shear modulus exponent, n_p	0.25
Peak friction angle, ϕ_F	35.5
Constant volume friction angle, ϕ_{cv}	33.0
Failure ratio, R_f	0.97
Factor of plastic anisotropic response, F	0.333

To simulate the element response in undrained and inflow states, the appropriate volumetric strain is applied by constraining the boundaries of the element. When analyzing an undrained state the volumetric strain increment ratio, $d\varepsilon_v/d\varepsilon_1$ is held equal to zero, while for a controlled flow test, the ratio is specified to match the value in the test to be simulated. Initially this was done by imposing a uniform radial strain rate on a single soil element.

The predicted response so obtained is compared to the test results for undrained; $d\varepsilon_v/d\varepsilon_1 = 0$, and inflow; $d\varepsilon_v/d\varepsilon_1 = -1$ states in terms of stress-strain relationship in Fig. 7. While a good agreement is obtained for an undrained test, the predicted response for the inflow test is softer than observed.

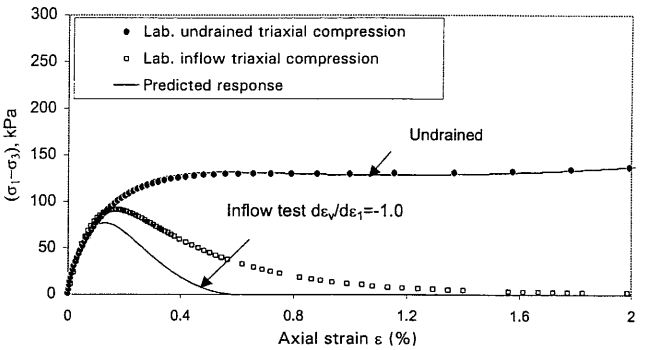

Fig. 7. Element response in undrained and inflow triaxial compression test on loose Fraser River sand; single element model

During inflow simulation using a single element, the volumetric deformations were assumed to be uniform, an assumption that is unrealistic due to the frictional constraints at top and bottom boundaries of the sample. These non-uniform deformations, even though very small, result in pore pressure redistribution within the soil sample that markedly affects its response.

To consider these non-uniform deformations, the soil sample was modeled by a multi-element grid in an axis-symmetric configuration and taking into consideration the friction at top and bottom boundaries. Friction effects were simulated by imposing lateral displacements at top and bottom boundaries of ¼ of the "free" values. The analysis was carried out in coupled stress flow mode to allow for pore water pressure redistribution. The specified volume change, $d\varepsilon_v$ was controlled by flow of water into the sample similar to that used in the physical sample.

The predicted stress strain response for the multi-element grid for undrained and inflow ($d\varepsilon_v/d\varepsilon_1 = -1$) conditions, is compared to the test results in Fig. 8a. The response in terms of pore pressure versus axial strain is compared in Fig. 8c and the stress path are shown in Fig. 8d.

A better agreement is obtained for the inflow test, while the predictions for an undrained state are almost the

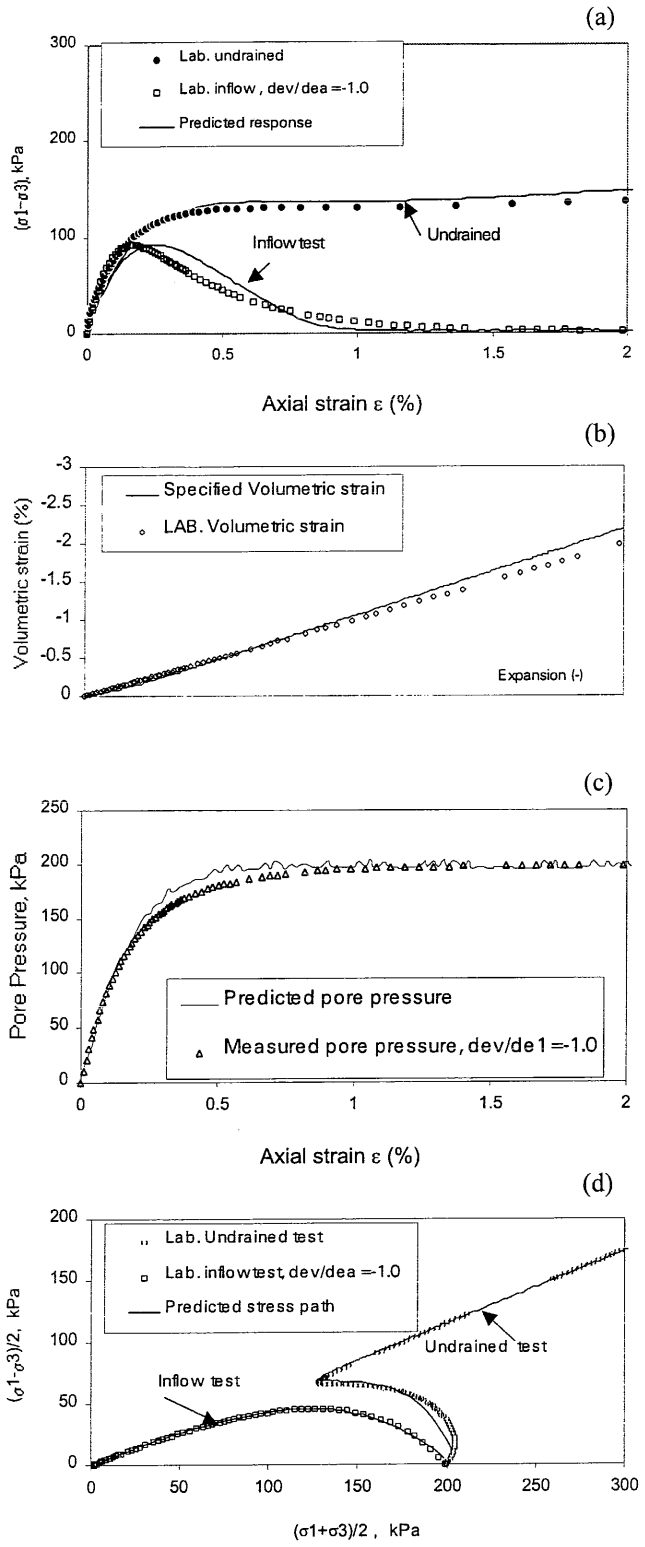

Fig. 8. Element response in undrained and inflow triaxial compression tests on loose Fraser River sand; multi-element model and (a) Stress strain response, (b) Specified volumetric strain, (c) Predicted pore pressure generated during inflow test loading, (d) Stress paths.

same as those obtained from single element analysis. This may be because at low strain levels, volumetric strains for an undrained test are extremely small, and hence the effect of non-uniform deformations becomes negligible.

In the field, elements may undergo a range of conditions from undrained, to inflow, to outflow, to fully drained. The predicted shear and volumetric response of loose Fraser River sand for this range is shown in Fig. 9. The laboratory verifying data are not shown for clarity but are in close agreement with the predictions shown. The response for drained or outflow tests are strongly strain hardening while the undrained test is mildly strain hardening and the inflow test is highly strain softening. Thus from Fig. 9, it may be seen that the shear response of sand is highly dependent on volumetric strains caused by local flow. Inflow or outflow to an element has an enormous effect on the shear response of sand, turning it from a strong strain hardening material under outflow, to a weak strain softening material under inflow conditions. The volumetric strains to bring about this transformation are very small, in the range of 1%.

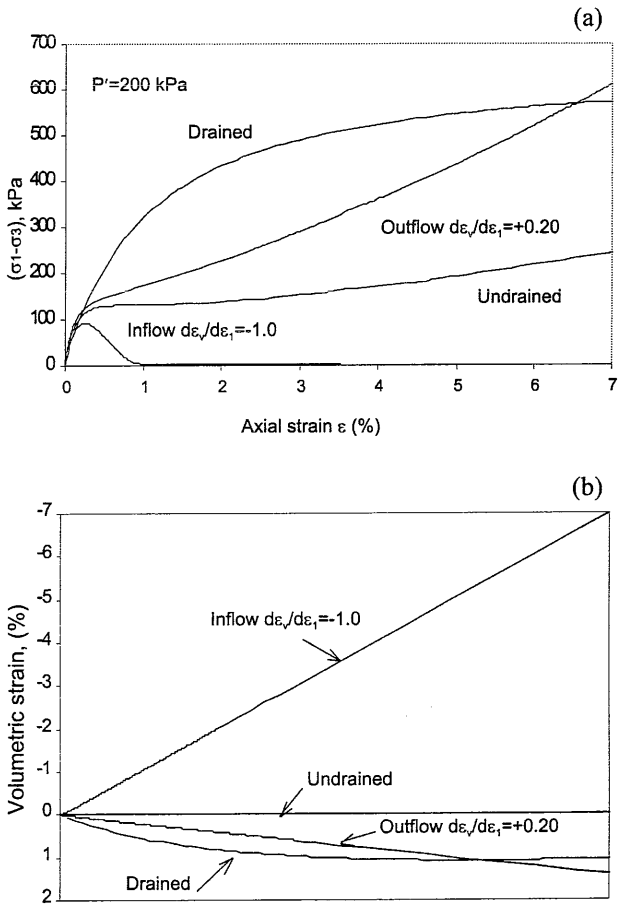

Fig. 9. Predicted element response in triaxial compression test of loose Fraser River sand for different degrees of drainage: (a) Stress-strain response, (b) Volume change.

Analysis of embankment

To investigate the effect of drainage condition on soil movements, an embankment subjected to surface loading is studied. The surface loading is applied rapidly so as to generate high excess pore pressures. Whether such excess pore pressures are generated by monotonic or earthquake loading, their dissipation will follow a similar pattern. They will be controlled by the boundary conditions and any internal low permeability layers.

The embankment material and its foundation are assumed to consist of loose Fraser River sand with element response over the range of drainage conditions from conventional drained to undrained to inflow states, as described in the previous section and captured by the model. The model parameters used in the analysis are the same as those obtained from the test data and listed in Table 1.The embankment is constructed in two stages as shown in Fig. 10. The first stage comprised of placement of material under a fully drained condition to a height of 18m above the foundation. The second stage comprised of placement of 5 meter of dry sand with a unit weight equal to 16 KN/m^3 on top of the previously constructed embankment. The geometry and boundary conditions of the numerical model are shown in Fig. 11. The water table is horizontal and at a depth of 8m. The rapid placement of the stage two material is first simulated assuming an undrained condition. Then redistribution of water with and without a drainage barrier is considered using a coupled stress flow analysis.

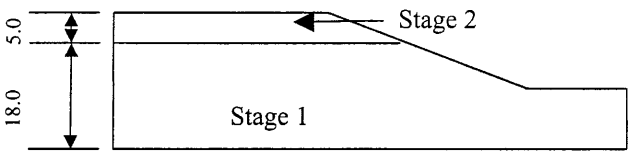

Fig. 10. Embankment Construction Stages

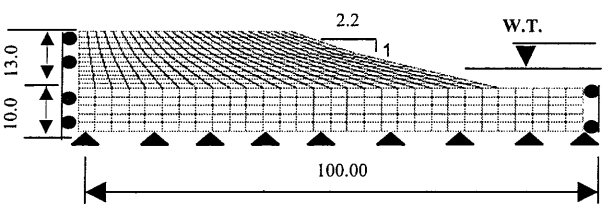

Fig. 11. Embankment, grid and boundary conditions

A fully drained condition was also considered. In this way undrained, partially drained and fully drained, conditions were examined.

The displacement pattern and contours of pore water pressure are presented in Fig. 12 for the undrained loading stage. A maximum displacement of about 0.6m is predicted (Fig. 12a). The contours of excess pore pressures (Fig. 12b) indicate high values of excess pore water pressure generated due to surface loading.

After the undrained stage, coupled stress flow analyses were performed to allow for redistribution and dissipation of excess pore water pressure. Here two assumptions were made regarding permeability of embankment material; (1) the embankment has homogeneous permeability, and (2) a horizontal barrier layer of low permeability exists at a depth of 8m. Base and vertical sides are "impermeable" boundaries. For both conditions, the generated pore pressure is allowed to dissipate.

Homogeneous permeability

Fig. 13 shows the displacement pattern at the end of dissipation as well as the flow vectors during dissipation for the embankment without an impermeable layer. Here both the sloping surface and the top surface of the embankment are considered as drainage boundaries while all other boundaries are assumed to be impermeable. The maximum displacement occurs in the toe area and is about 0.9m, an increase of about 50% from the undrained condition.

Drainage barrier

The barrier layer condition is shown in Fig. 14. The upward flow of water is constrained by this boundary and is redirected toward the slope surface, which is the only free draining boundary. Flow vectors during dissipation of pore water pressure (Fig. 14b) shows this phenomenon. Displacement pattern for this case (Fig. 14a) is similar to that for the undrained case, but displacements have increased to 3.2m after 20 sec and continue to increase with time.

Pore pressure and volumetric changes in an element below the drainage barrier (Fig. 15) are shown in Fig. 16. It may be seen that the barrier curtails drainage causing in- flow into the element (Fig. 16b) and pore pressure rise (Fig. 16a). This in turn causes the element to loose resistance and large strains to build up beneath the barrier resulting in the predicted large displacements. These strains are occurring under essentially constant shear stress arising from the sloping ground and increase with time as inflow into the element occurs. A flow failure takes place when the resistance drops below the driving stress.

Loading under drained conditions results in no excess pore water pressure. The predicted displacements are shown in Fig. 17 and are small (a maximum of 0.05m) compared to displacements of about 1 m for undrained conditions (Fig. 17).

a) Displacement vectors,
Maximum vector = 0.6m.

b) Excess pore pressure contours,
Contour interval = 25 kPa

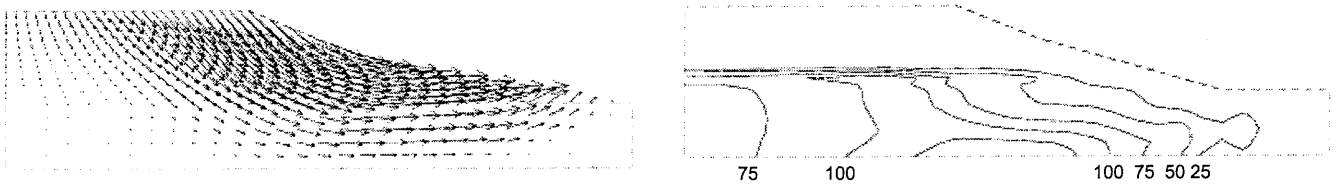

Fig. 12. Undrained response under placement of fill material: (a) Displacement vectors, (b) Contours of excess pore pressure

a) Displacement vectors,
Maximum vector = 0.9m.

b) Flow vectors during dissipation of excess pore water pressure

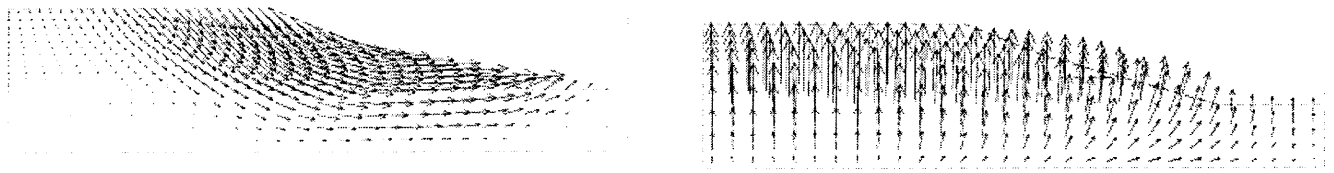

Fig. 13. Embankment without an impermeable layer: (a) Displacement vectors, (b) Flow vectors during dissipation of excess pore pressure

a) Displacement vectors,
Maximum vector = 3.25m.

b) Flow vectors during dissipation of excess pore water pressure

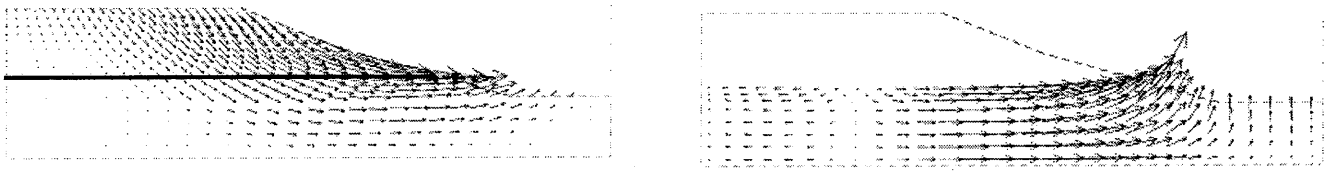

Fig. 14. Embankment with an impermeable layer: (a) Displacement vectors, (b) Flow vectors during dissipation of excess pore pressure.

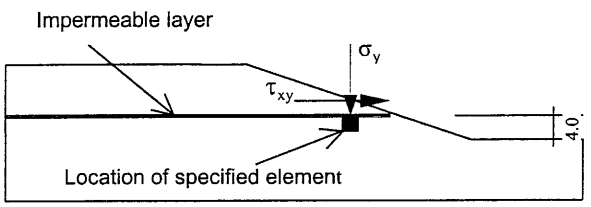

Fig. 15. Location of specified element in embankment.

Implications for lifelines

In many areas of the world, lifeline structures traverse soil deposits that are susceptible to liquefaction. This is particularly the case for the Lower Mainland of British Columbia, where bridge and pipeline structures are supported in or on recent alluvial and deltaic deposits.

The loss in soil resistance and the large soil displacements that can arise from liquefaction may result in large and damaging displacements of the lifeline structure. Many of the existing bridges and pipelines are being analyzed for such effects and remedial measures including soil densification designed.

The standard procedure is to base the liquefaction design on the assumption that no drainage occurs during the few seconds of strong shaking that could trigger liquefaction. It is not unreasonable to assume that no significant drainage would occur during this period. However, in the period after the shaking, drainage or movement of water may very well occur. It has generally been assumed that such drainage would lead to reduced pore pressures, a reduction in volume and increased strength as excess water escaped. However, if drainage is curtailed by the presence of low permeability horizontal

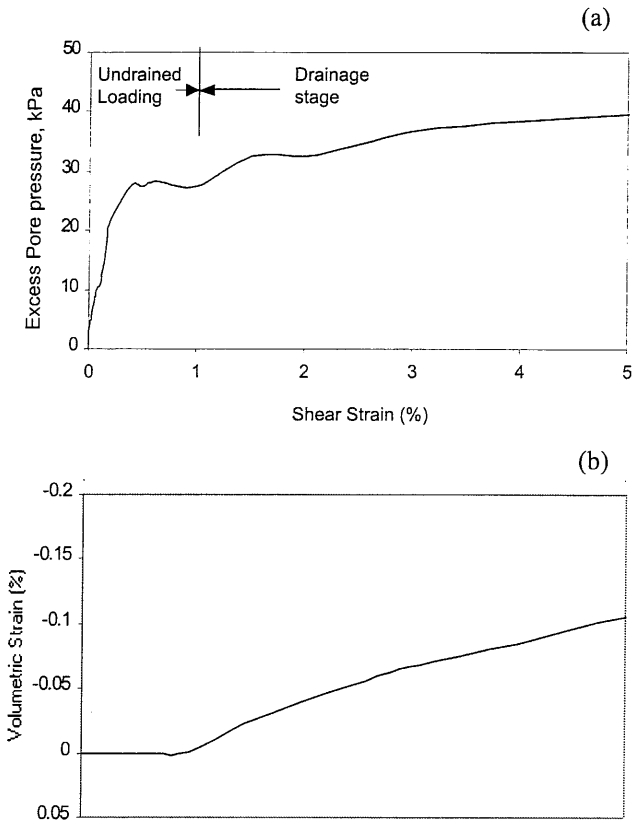

Fig. 16. Element response in liquefied zone of embankment with an impermeable layer: (a) Pore pressure response, (b) Induced volumetric strain.

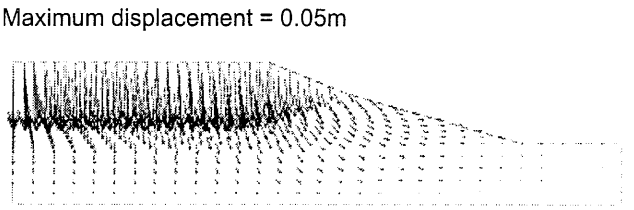

Fig. 17. Embankment behavior under drained loading; displacement vectors

layers, an accumulation of water and increased porewater pressures at the base of such layers can occur. Recent laboratory test data suggest that inflow of only a very small amount of water into a sand element can greatly reduce its resistance causing it to behave in a strain softening manner. Such behaviour can occur even in a dense sand that would normally be expected to dilate.

In this paper, the effect of such inflow was examined numerically. The test or element behaviour of Fraser River sand over a wide range of loading from drained to undrained to inflow was captured in an elastic plastic model. The model was then applied to an embankment situation and the effect of drainage evaluated. It was shown that the presence of a horizontal layer of low permeability impedes drainage causing the element to expand and the pore pressure to rise as it shears. This can result in strains and displacements well in excess of the undrained response.

Shake table tests reported by Kokushu (1998) confirm this behaviour. In his tests, the accumulation of water at the interface was so great that a water film or bubble was observed beneath the base of the low permeability barrier layer followed by a flow slide.

The flow slide that occurred on the upstream slope of the Lower San Fernando dam following the 1971 San Fernando earthquake was due to a reduction in strength most likely caused by inflow into critical zones related to the layered nature of the materials of the dam.

Many soil profiles in the Lower Mainland have a distinct low permeability silt cap layer overlying liquefiable granular soils. Accumulation of water at the base of such a cap during or after strong ground shaking is likely to occur and should be considered in remedial measures by the provision of adequate drainage.

While many densification schemes do include drainage by way of high permeability stone columns, the quantity of water to be removed in a short time can be quite high and enhancement by the addition of slotted pipes may be necessary.

References

Beaty, M.H. and Byrne, P.M. 2000. A synthesized approach for predicting liquefaction induced displacements, selected for Oral Presentation at the 12th World Conference on Earthquake Engineering, Auckland, New Zealand, Jan. 20 to Feb. 4, 2000.

Beaty, M. and Byrne, P.M. 1999. A simulation of the Upper San Fernando dam using a synthesized approach, Proceedings of the Symposium on Slope Stability and Landslides, Vancouver Geotechnical Society, Vancouver, Canada, May 28.

Byrne, P.M., Phillips, R. and Zang, Y. 1995. Centrifuge tests and analysis of CANLEX field event. 48th Canadian Geotechnical Conf., 353-366, Vancouver, B.C. September.

Cundall, P. 1998. FLAC User's Manual, Version 3.4, ITASCA Consulting Group Inc., Minneapolis, USA.

Eliadorani, A.A. 2000. The response of sands under partially drained states with emphasis on liquefaction, Ph.D. Thesis, University of British Columbia, Vancouver, Canada.

Kokushu, T. 1998. Water film effect on lateral spreading in liquefied sand, video tape presented at Proceedings of Geotechnical Earthquake Engineering and Soil Dynamics Conf., ASCE, Seattle, Washington, August.

Puebla, H., Byrne, P.M. and Phillips, R. 1997. Analysis of Canlex Liquefaction Embankments: Prototype and Centrifuge Models, Canadian Geotechnical Journal, Vol. 34, No. 5, pp. 641-657.

Puebla, H. 1999. A constitutive model for sand and the analysis of the CANLEX embankments, Ph.D. Thesis, University of British Columbia, Vancouver, Canada.

Vaid, Y.P. and Sivathayalan, S. 1998. Fundamental factors affecting liquefaction susceptibility of sands, Keynote lecture at the International Workshop on the Physics and Mechanics of Liquefaction, Sept. 10-11.